Identification of thermo-viscoplastic behavior for AA6061 under in-plane biaxial loadings

J Liang, Dominique Guines, Lionel Leotoing

J. Liang[1], D. Guines[2*], L. Leotoing[2]

[1] *Key Laboratory of Intelligent Machining Technology and Equipment, Fujian University of Technology, Fuzhou 350118, China*

[2] *Univ Rennes, INSA Rennes, LGCGM (Laboratoire de Génie Civil et Génie Mécanique) - EA 3913, F-35000 Rennes, France*

**corresponding author's email: dominique.guines@insa-rennes.fr*

Identification of thermo-viscoplastic behavior for AA6061 under in-plane biaxial loadings

Abstract

This work aims to investigate the thermo-visco-plastic behavior of an aluminum alloy (AA6061) sheet metal submitted to in-plane biaxial loadings under warm conditions. Biaxial tensile tests are performed in a temperature range from room temperature to 160°C, and in a strain rate range from quasi-static to the so-called "intermediate" strain rate (up to few s^{-1}). The specimen shape used in this study has been previously defined and validated by the authors to identify the viscoplastic hardening models of metallic alloys at large strains. A specific device leading to a uniform temperature in the sample is associated with a dynamic biaxial traction bench to carry out the temperature and strain rate dependent characterizations. From these experiments, both the experimental forces measured on each axis of the in-plane biaxial specimen and the principal strains at the center of the specimen are obtained. These experimental data are then used in an inverse analysis loop, based on a finite element model of the biaxial test, to calibrate the parameters of a thermo-viscoplastic strain hardening model by minimizing the difference between the experimental and numerical principal strains at the center point of the specimen. Finally, it is shown that the identified hardening model well predicts the flow stress of AA6061 under different temperatures and strain rates for a strain level of up to 40%.

Keywords:

In-plane biaxial tension; Temperature-dependent behavior; Intermediate strain rate; Strain hardening; AA6061.

1 Introduction

Simulation of hot forming processes requires the calibration of rheological models in appropriate strain rate and temperature ranges. In the characterization field of mechanical properties of metal sheets, the in-plane biaxial tensile test on cruciform specimen is increasingly used and presents several benefits compared to the conventional testing methods. First of all, this test makes it possible to reach higher levels of deformation than those classically obtained by the traditional uniaxial tensile test. Moreover, for thin products such as metal sheets, this test allows to apply loading conditions close to those encountered during the forming process. Compared to the Marciniak or Nakazima stamping tests, often used to characterize the sheet metal formability, the biaxial tensile test on flat cross-shaped specimens presents the advantage of being frictionless without any contact between the tested specimen and any tooling. Depending on the specimen shape, different strain or stress states ranging from uniaxial tension to biaxial tension can be observed during a unique test in different regions of the specimen. Finally, by changing the displacement ratio applied to the two axes of the cross specimen, different linear or non-linear biaxial strain paths can be obtained at the central point of the specimen [1]. Over the last ten years, a growing interest has developed around the use of this original test, applied in particular to the study and characterization of different behaviors of metal sheets such as: (i) the determination of initial yield locus for isotropic or anisotropic materials [1–6]; (ii) the identification of hardening models [3,7–10]; (iii) the determination of forming limit curve at necking (FLCN) or forming limit curve at fracture (FLCF) [11–17]. The major difficulty in carrying out this test, always lies in the definition of an appropriated specimen geometry and, as can be seen in the literature, a large number of specimen shapes have been proposed, depending on the targeted application. Recently, a standardized geometry of cruciform specimen [18] was proposed on the basis of the work of Kuwabara [2]. Nevertheless, this specimen shape only allows to reach low levels of deformation and finds its main application in the determination of initial yield surfaces. Therefore, to achieve large strains other shapes are more adequate [8].

In sheet forming processes where improved formability is targeted, temperature and strain rate are two essential factors whose influence must be taken into account, especially for aluminium alloys with poor formability at room temperature. The characterization of the mechanical behavior of sheet metal both in temperature and for different strain rates from a biaxial tensile test on an in-plane specimen is still rather uncommon to date. Abu-Farha et al. [19] performed quasi-static in-plane biaxial tensile tests on different materials (AA5083, MgAZ31b and twinning induced plasticity steel), using a heat gun to generate a localized heating of the gauge area of the specimen. A maximum temperature of around 350°C is reached in the specimen's gauge area with this device. Kulawinski et al. [20] designed an inductive heating system installed on a servo-hydraulic biaxial planar tension-compression machine. The fatigue behavior of a forged nickel-base superalloy Waspaloy™ was investigated at temperatures of 400°C and 650°C with a strain rate of $10^{-3}s^{-1}$. Both of these processes directly heat the center area of the specimen, preventing high-temperature damage to test equipment parts such as the chuck, pull rod and related sensors. However, a non-homogeneous temperature distribution on the specimen is obtained which does not simplify the calibration procedure of behavior models. Shao et al. [21] developed a heating system based on the Joule effect. With this heating method, biaxial tensile tests were performed and experimental forming limit curves are obtained for AA6082 at temperatures of 400 and 500°C and strain rate of 0.1/s. Finally, the

author concluded that, this method can be used to determine the hot formability of sheet metal up to maximum temperatures of 1000°C. Nevertheless, this heating technique does not seem to provide a homogenous temperature field in the specimen. To solve this problem, the isolated box containing the specimen inside is an efficient method to reach a homogeneous temperature on the whole specimen. Using this heating method, Xiao et al. [22] designed a heating furnace for an in-plane biaxial tensile test to study the behavior of a GH738 nickel-based superalloy. Experiments were performed under three different temperatures (20, 300, and 500°C) and different tensile velocity ratios (0.02mm/s on each side; 0.03mm/s on the X-axis and 0.02mm/s on the Y-axis). Nevertheless, all the thermal in-plane biaxial tensile tests presented above are carried out under quasi-static conditions (around 10^{-3}/s to 0.1/s), and to the best of the authors' knowledge, no study proposes temperature characterizations from biaxial tests on flat cruciform specimens for intermediate or high strain rates.

In this study, the tested material is an aluminum alloy 6061 (AA6061-O), widely used to produce structural components in automotive, aircraft and marine industry because of its high strength to weight ratio and excellent corrosion resistance [23,24]. Fan et al. [25] investigated the dynamic mechanical behavior of AA6061 at different temperatures (20 to 400°C) and different strain rates (10^{-3} to $10^{4}s^{-1}$). The results indicate a significant temperature effect on the strain hardening for this material, while the strain rate effect is more obvious at relatively high temperatures (300 to 400°C) than at low temperatures. Chen et al. [26] evaluated the effect of temperature (ambient to 380°C) and strain rate (0.0005 to $0.05s^{-1}$) on the formability of AA6061-T6. The experimental results show that the forming limits of this material increased with the increasing temperature and the decreasing forming speed. Khamei et al. [27] studied the deformation of AA6061 at temperatures of 300°C, 400°C, and 500°C and for strain rates ranging from 0.0005 to $0.01s^{-1}$. The authors concluded that the thermo-mechanical behavior of AA6061 is strongly dependent on temperature and strain rate, i.e., the flow stress increases with increasing strain rate and decreasing temperature. In the study of Kacem et al. [28], the temperature influence on the ductile fracture behavior of AA6061-T6 aluminum alloy was investigated from room temperature to 200°C under different stress states by means of tensile tests performed on different specimen shapes. Authors claim that the fracture strain is strongly dependent on the temperature and also stress state. It is also found that the temperature effect on the stress triaxiality is rather small and depends on the specimen geometry. Based on hot compression at temperatures of 400, 450, 500 and 550°C and strain rates of 0.1, 1 and $10s^{-1}$, Rudnytskyj et al. [29] studied the mechanical behavior of AA6061 during the hot rolling process and identified the material model over a wide range of strains up to 1. Through the literature results, it is obvious that the behavior of AA6061 alloy (strain hardening, formability), shows a non-negligible sensitivity to temperature and strain rate.

In order to accurately describe the hardening behavior of the material, an appropriate hardening model should be selected by considering the temperature and strain rate ranges. In the literature, several studies have focused on characterizing the strain hardening of AA6061 as a function of temperature and strain rate [30-34]. However, these have mainly focused on high strain rates (up to $10^{4}s^{-1}$). The modification of the original Johnson-Cook (J-C) model has been widely used to describe this behavior while this type of hardening model is not adapted for quasi-static conditions and for the so-called "intermediate" strain rate regime. Roy et al [35] studied the plastic deformation of AA6061-T6 alloy at temperatures ranging from room temperature to 500°C under quasi-static conditions (0.00125/s and 0.00167/s). The author states that strain rate effects cannot be neglected above 150°C for this material. Therefore, in order to describe the influence of strain rate on the hardening behavior of AA6061 at elevated temperature, a hybrid Swift/Voce law combined with a J-C strain rate dependence form was used. The result shows that this model can well reproduce the full field characteristics of the high temperature experiments. In [36], the Zerilli-Armstrong model was used to describe the impact of temperature on the microstructure evolution of AA6061-T6 at temperatures ranging from 100 to 350°C and for dynamic conditions ($10^{3}s^{-1}$). The author states that the stress-strain response of face centered cubic (FCC) alloys such as AA6061-T6 can be well described by the Zerilli-Armstrong model in these temperature and strain rate ranges. Vilamosa et al. [37] studied the thermo-mechanical behavior of AA6XXX over a wide range of temperature (20-350°C) and strain rate ($0.01-750s^{-1}$). A physics-based model, the Voyiadjise-Abed one, was introduced to describe the stress-strain behavior of the alloys. From the results, the hardening model can generally reproduce the rheological behavior of these materials at different temperatures and strain rates, but in some cases, there are also significant discrepancies between the numerical and experimental data. For an AA5086, Chu et al. [30] study the influence of material thermo-viscoplastic models on the predicted FLCs by a finite element M-K model. The flow stresses were characterized by uniaxial tensile tests at different temperatures (20, 150, and 200°C) and equivalent strain rates (0.0125, 0.125, and $1.25s^{-1}$). Three types of hardening models (power law model, saturation model, and mixed model) were proposed and adapted to correlate the experimental flow stresses. Results show that the predicted limit strains were very sensitive to the thermo-viscoplastic modeling.

In this study, a calibration method of thermo-viscoplastic hardening models of an aluminium alloy AA6061-O based on an in-plane biaxial tensile test is proposed. The calibration methodology developed these lasts years in the team to characterize the strain-rate dependency of metallic alloys under in-plane biaxial loadings [8, 9, 32] at ambient temperature is extended in order to integrate the temperature dependency. The heating device adopted here is an air flow generator coupled with and insulated box allowing to achieve a homogeneous temperature fields, for different set-point temperatures on the in-plane cross specimen. Temperatures ranging from ambient to 200°C are controlled by this heating set-up and the 4-hydraulic actuators of the in-plane biaxial bench

allow to perform tests from quasi-static conditions to intermediate strain rates (up to few ten of s^{-1}). The sensitivity of the material behavior with respect to temperature and strain rate has been first highlighted from uniaxial tensile tests in a preliminary work [34]. On the basis of this previous work, an appropriate formulation for a thermo-viscoplastic strain hardening model has been selected and calibrated. Results show that the chosen model is suitable for reproducing the sensitivity of the AA-6061 material to temperature and strain rate within the chosen ranges of variation. Thereafter, on the same temperature and strain rate ranges, equi-biaxial tensile tests are performed on a dedicated flat cruciform specimen of AA6061-O. A parameter calibration of the thermo-viscoplastic strain-hardening model previously chosen in [34] is then proposed by means of an inverse procedure based on both a FE model of the equi-biaxial tensile test and the experimental data. The identified biaxial flow stress curves are then compared between different conditions to show the temperature and strain rate dependency on the hardening behavior of AA6061 for large strains.

2 Experimental in-plane biaxial tensile tests at different temperatures and intermediate strain rates

2.1 Experimental setup

The material investigated is the aluminum alloy 6061-O provided in sheets of initial thickness 2 mm with a chemical composition as given in Table 1.

Table 1 Chemical components of AA6061-O in weight percent.

Component	Wt. %	Component	Wt. %	Component	Wt. %
Al	95.8-98.6	**Mg**	0.8-1.2	**Si**	0.4-0.8
Cr	0.04-0.35	**Mn**	Max 0.15	**Ti**	Max 0.15
Cu	0.15-0.4	**Other, each**	Max 0.5	**Zn**	Max 0.25
Fe	Max 0.7	**Other, total**	Max 0.5		

As outlined in section 1, in the last decade, a specific in-plane biaxial tensile device (**Fig. 1**) has been intensively used to investigate different mechanical behaviors for metallic materials under static and dynamic biaxial loadings [16,31,32] at room temperature. Experimental tensile forces are measured by strain gauge sensors (one on each axis). For the dynamic tensile tests, the additional masses are accelerated along the sliding bars to obtain the required velocity before the specimen is loaded, then the specimen is suddenly impacted and the velocity is maintained during the test due to the inertia effect of the additional mass [8].

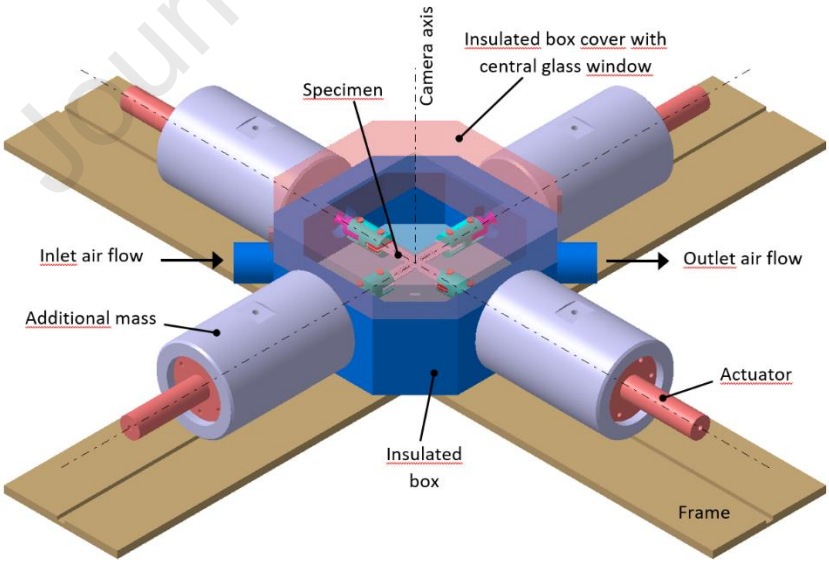

Fig. 1 Cruciform specimen positioned in the center of the biaxial experimental device with an insulated box [8]**.**

The heating device consists in an airflow generator supplying an insulated box as shown in Fig. 2a. The allowed temperature range of the air flow generator is from -75°C to 200°C. The generated hot air is flowed into the insulated box through an inlet pipe and then return to the airflow generator through an outlet pipe. For a given set-point temperature, the temperature of the hot air sent by the air generator is regulated from the temperature measured inside the chamber by a remote probe. For each temperature tested,

a verification test is first carried out by instrumenting a specimen with a thermocouple placed in the center of the specimen and another positioned on one arm of the specimen. These thermocouples allow to verify, when the tensile test is launched, both the homogeneity of the temperature and the value of this temperature in the specimen when the targeted temperature is reached in the insulated chamber. Since the heating is relatively slow (approx. 1 hour for 160°), these two aspects are clearly verified (by the thermocouple measurement), nevertheless, when the target temperature is reached, a 10-minute temperature hold is applied before the tensile test.

A high-speed camera (Photron FASTCAM-APX RS) is placed on the central axis (Fig. 1a and Fig. 2a) of the biaxial bench to capture successive images of the specimen during the tensile stage, through the glass pane on the top of the insulated box. The specimen is lighted from the outside, at the level of the glass window, by four strands of light directed towards the central area of the specimen (see detailed Fig. 2b).

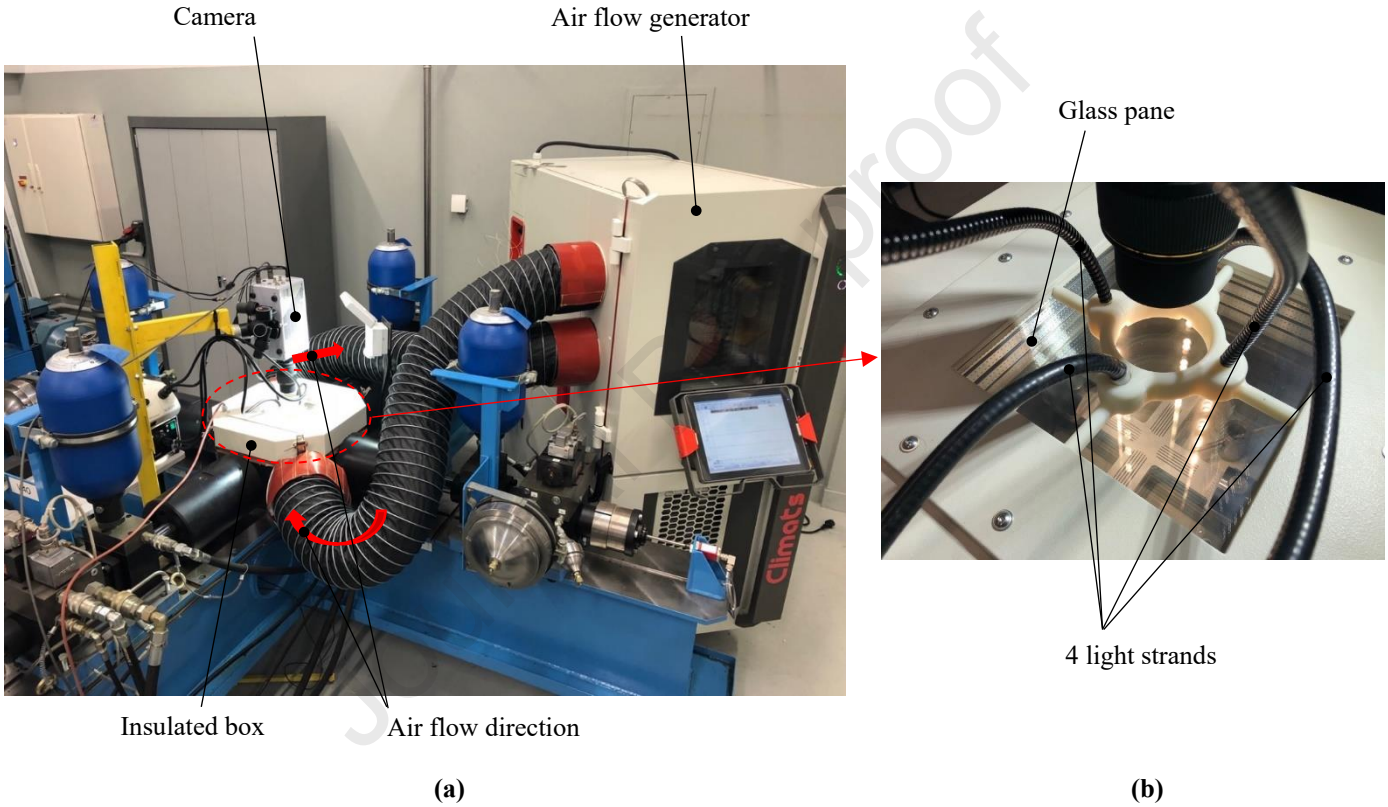

Fig. 2 Biaxial tensile machine equipped with heating device.

The shape of the cruciform specimen (Fig. 3) proposed by Liu et al. [8] is adopted in this study. Large equivalent plastic strains (up to 30% of equivalent plastic strain) in the central zone under equi-biaxial tensile loadings, for quasi-static or dynamic conditions, are obtained with this shape. This specimen shape has a single thickness reduction, made in the center of the specimen, where the initial 2 mm sheet thickness is reduced to 0.625 mm. The X-axis corresponds to the transverse direction, and the Y-axis corresponds to the rolling direction.

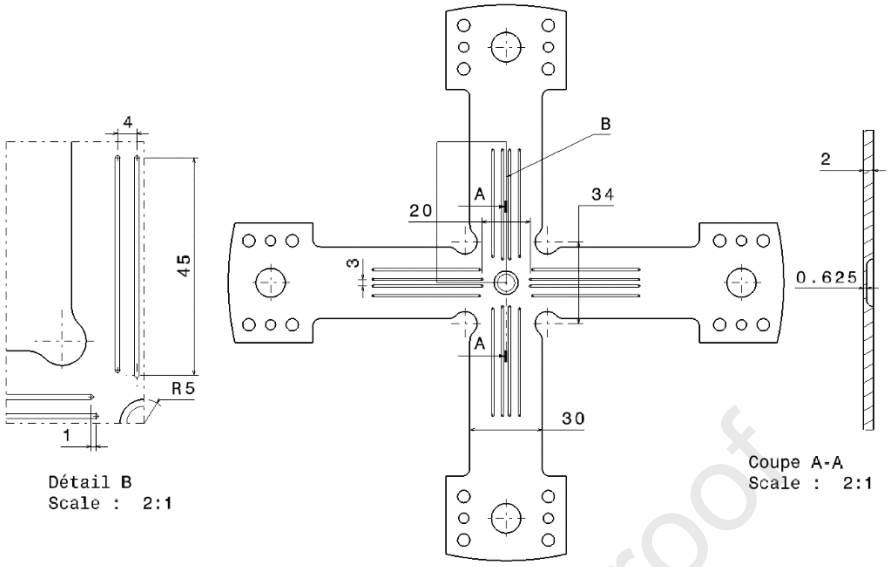

Fig. 3 Cruciform specimen shape for in-plane biaxial tensile test.

2.2 Experimental results of biaxial tensile tests

Two experimental quantities are used thereafter in the identification procedure of the strain-hardening behavior of the studied material: the equivalent plastic strain at the center of the specimen and the tensile forces on the two perpendicular axis of this same specimen.

Strains at the specimen surface are calculated by DIC technique with GOM Correlate software. Since specimens are not symmetrical in thickness as it can be seen in Fig. 3, it was chosen to generate the random speckle pattern on the flat side of the specimen before the tests (Fig. 4a). After the tests, the correlation stage is performed with subsets of 32 pixels × 32 pixels, offset by 16 pixels from each other. The magnification factor is 0.037mm/pixel. The gauge area treated by DIC is around 15mm square area with 720 analysis points as the blue area in Fig. 4b. The black circle of diameter 7.25mm corresponds to the central zone of 0.625mm constant thickness of the specimen. The experimental evaluation of the total equivalent strain, in the von Mises sense, at the central point of the specimen is obtained by the average value as follows:

$$\varepsilon(t) = \frac{1}{m \times n} \sum_{j=1}^{m} \sum_{i=1}^{n} \varepsilon(i, j, t) \tag{1}$$

where m and n are the number of points to be averaged along X and Y directions, respectively, and t is the time. In this work, the average strains are calculated over the 2×2 points, which corresponds to a square area of 0.5mm side at the center of the specimen corresponding to the red square in Fig. 4.

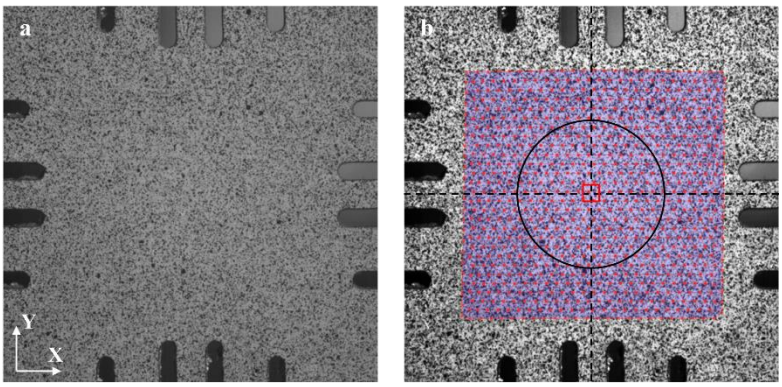

Fig. 4 Central zone of the specimen; (a) Speckle pattern; (b) Area processed by image correlation (Purple square area), area of constant thickness (black circle), and average area (red square).

Equi-biaxial tensile tests are performed at 20°C, 100°C, and 160°C for tensile speeds of 0.02mm/s, 2mm/s and 200mm/s. These velocities are applied at each end of the 4 arms of the tested specimen. The tensile force (along the rolling direction, i.e. Y-axis) curves versus the equivalent plastic strain at the specimen center are presented below (Fig. 5) to observe potential material sensitivities to temperature and strain rate under equi-biaxial tensile loadings.

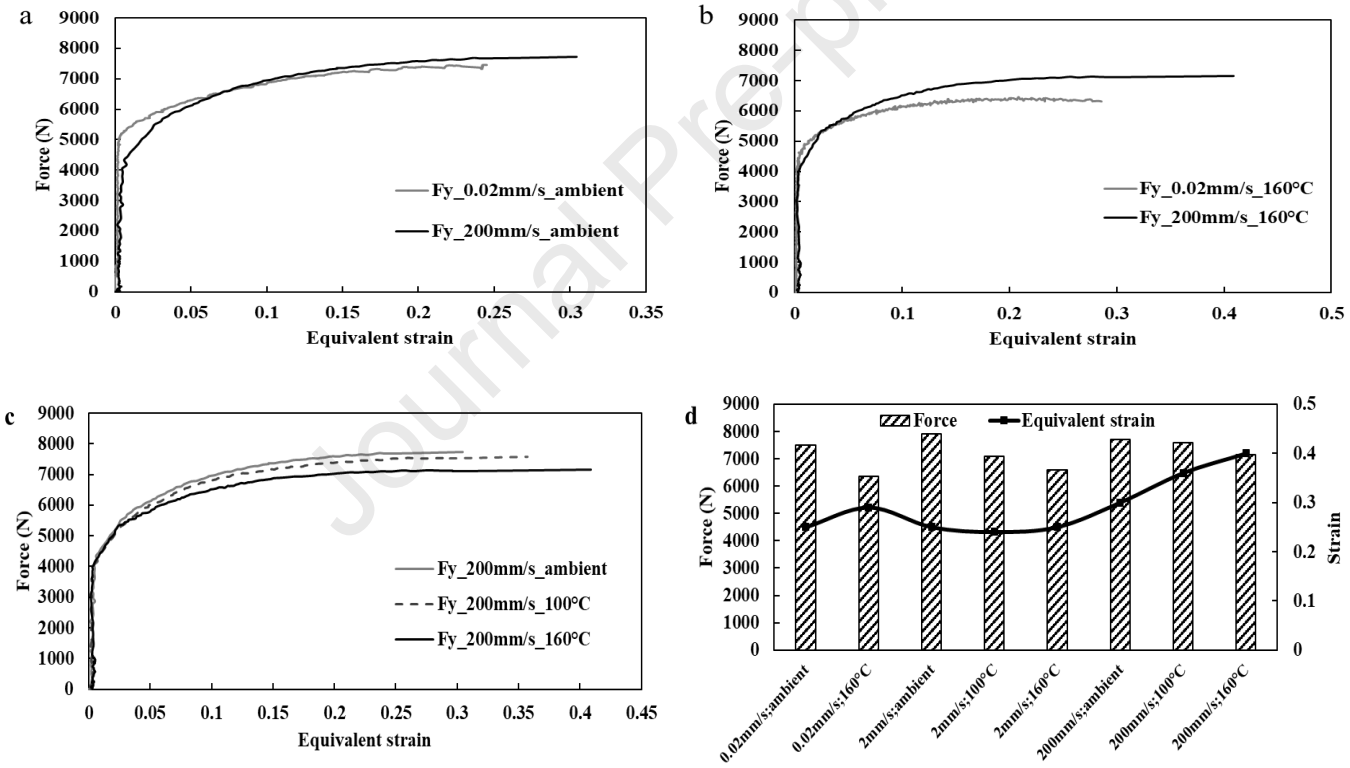

Fig. 5 Experimental forces along rolling direction versus equivalent strain at the specimen central point for biaxial tensile tests :
a) at ambient temperature ; b) at a temperature of 160°C ; c) at ambient temperature, 100°C and 160°C for a testing speed of 200 mm/s ; d) Maximum forces along the rolling direction and maximum equivalent strain for all the experimental tested conditions.

In Figure 5a and 5b, the forces along the Y-axis (rolling direction) are compared for quasi-static and dynamic conditions at ambient and 160°C, respectively. As expected, based on the maximum experimental force, the influence of tensile velocities on the strength at room temperature can be regarded as negligible (Fig. 5a), while a positive strain rate sensitivity is observed at 160°C between the conditions 0.02mm/s and 200mm/s (Fig. 5b) which corresponds to an increase of around 10% of the maximum load. For the tensile speed of 200mm/s in Figure 5.c, a negative effect of the temperature on the tensile strength clearly appears with a

decrease of approximately 8% of the maximum load between respectively the ambient temperature and the maximum one. The maximum forces along the rolling direction (Y-axis) for all the experimental tested conditions are presented in Fig. 5d. At the same tensile speed, the tensile strength decreases with the increasing of temperature for both quasi-static and dynamic conditions. Within the range of the tested strain rates, no clear trend is observed at room temperature, so no relevant strain rate can be assumed at this temperature. A small positive strain rate sensitivity can be observed at 160°C between the conditions 0.02mm/s, 2mm/s and 200mm/s and the same trend seems to be found at 100°C between the two conditions tested. The maximum equivalent strain (according to von Mises), calculated at the central point of the specimen, are presented, Fig. 5d, for the image just before rupture. For the two lowest velocities (0.02 and 2mm/s), no clear trend emerges on the level of strain at failure whatever the tested temperature. At 200mm/s, the maximum equivalent strain increases gradually with increasing temperature (up to 40%), which has also been observed in other researches [27,33].

For the condition (200mm/s ; 160°C), the equivalent, major and minor strain fields in the specimen gauge area at time 0.0108s are presented in Fig. 6a, b, and c, respectively. The red circle is corresponding to the thickness reduction zone (diameter of 10*mm*). X-Axis corresponds to the transversal direction, Y-axis corresponds to the rolling direction. As explained above, the equivalent and principal strains at the central point are calculated by the strain average on four points defined in a square area of 0.5mm side (Fig. 4). This figure shows that the equivalent and principal strains are concentrated and nearly homogeneous in the specimen's central zone.

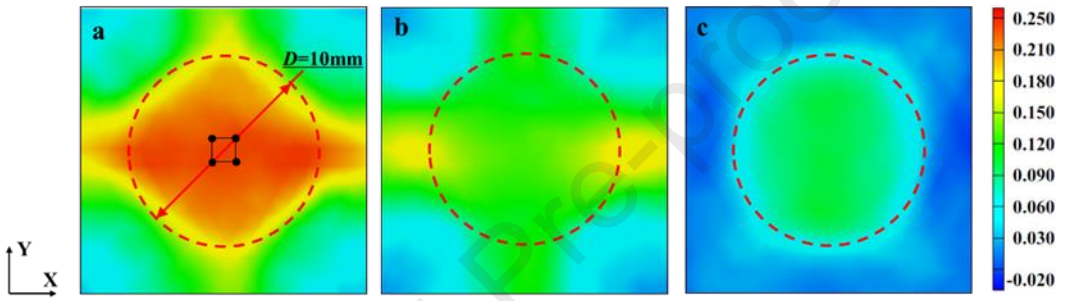

Fig. 6 Strain fields at 200mm/s and 160°C: (a) Equivalent strain; (b) Major strain; (c) Minor strain.

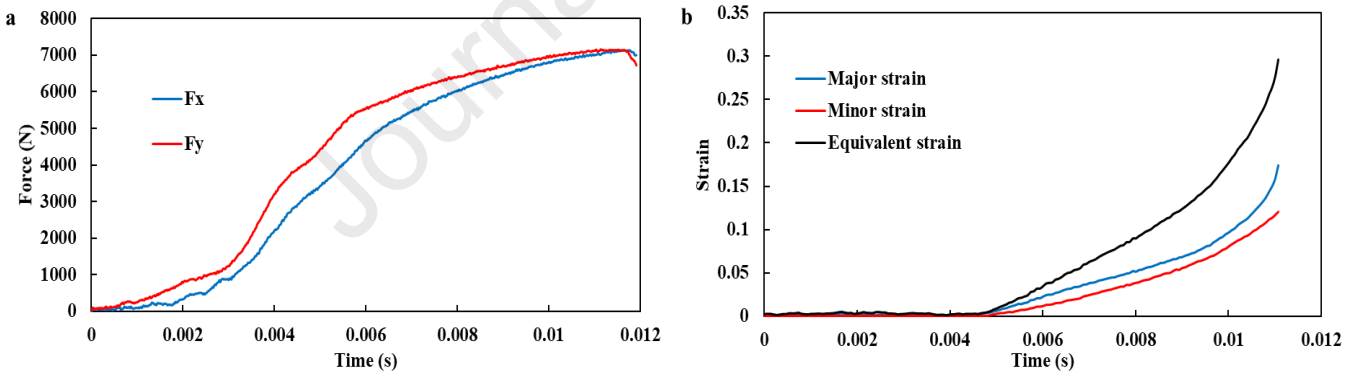

Fig. 7 Temporal evolution of tensile forces and strains for condition 200mm/s and 160°C : (a) Experimental forces ; (b) Equivalent and principal strains evolutions at the central point.

The evolution of experimental forces versus time is shown in Fig. 7a. A small discrepancy is observed between the experimental forces along the X and Y directions. Concerning the in-plane strains calculated at the central point of the specimen, the maximum equivalent strain reaches 30%, while the maximum major and minor principal strains are respectively about 17% and 12% (Fig. 7b).

The discrepancy observed between the experimental forces along the two axes of the specimen and that observed between the major and minor principal strains at the center of the specimen are due either to the desynchronization of the actuators, or to the anisotropic nature of the material, or to both. As a result, the strain path calculated at the center of the sample in this case is no longer equi-biaxial, as shown in Fig 8.

The strain path and equivalent strain rate evolution in the central zone of specimen for condition 200mm/s and 160°C are shown in Fig. 8. The strain path varies from 0.4 at the beginning of the test to a value of 0.8 at t = 0.009s, which corresponds approximately to the onset of necking, as shown by the fast increase of the strain rate from this point. A strain path equal to 1.0 can

only be achieved at the center of the sample if the imposed stress path is equi-biaxial and the material exhibits isotropic behavior.

During the test, the strain rate for these particular conditions (200mm/s and 160°C) fluctuates around $30s^{-1}$ at the center of the specimen (between t = 0.005s and t = 0.009s).

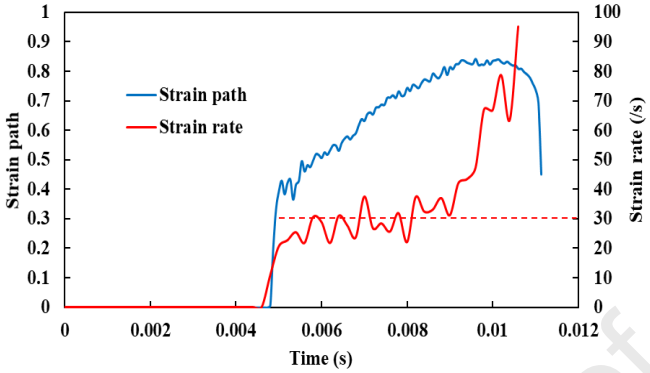

Fig. 8 Strain path and strain rate evolution at the central point for condition 200mm/s and 160°C.

To validate the repeatability of the experimental procedure, the results obtained for two tests performed at the same temperature and speed set points (160°C and 200mm/s respectively) are presented in Fig. 9. The comparison of measured experimental forces and calculated principal strains at the central point of the specimen is shown in Fig. 9a and Fig. 9b respectively. As can be seen from the time evolutions presented in Fig. 9, the results obtained show a rather good repeatability. As explained in section 4, the inverse procedure for calibrating the chosen hardening model is based on the time evolution of major and minor strains at the center point of the specimen. If the boundary condition of the equi-biaxial tensile test was perfectly applied during the test, which requires perfect synchronization of the four actuators of the biaxial bench, major and minor strains would be identical, and principal directions would in this case be the tensile X and Y directions. However, since the four actuators are never perfectly synchronized, the temporal evolution of the strains measured along the X and Y directions are not exactly the same. Major and minor principal strains differ in this case, and the principal directions no longer correspond exactly with the X and Y tensile directions.

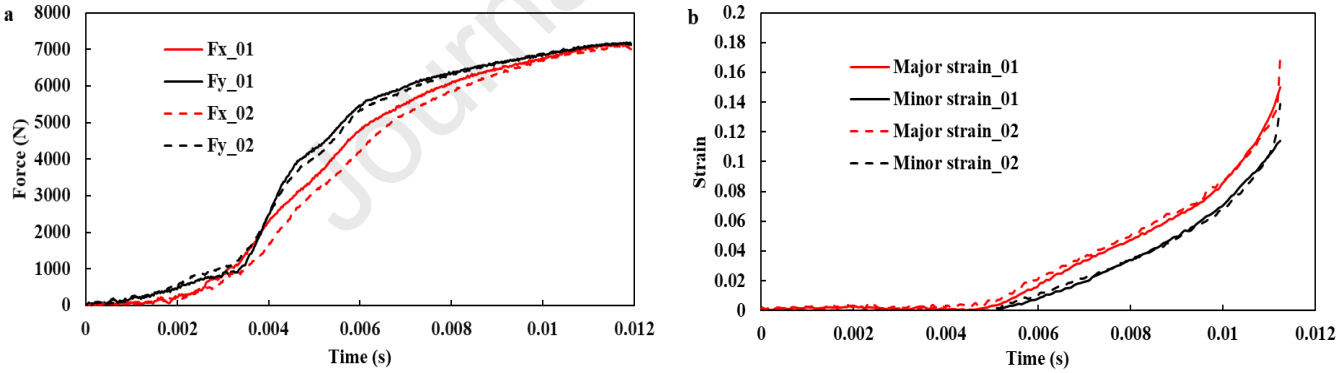

Fig. 9 Checking the repeatability for the condition 160°C and 200mm/s.

The complexity of the cross-shaped specimen adopted in this study (Fig. 3) leads to non-homogeneous fields of strain, strain rate, stress and temperature within the specimen. Since it is not possible to establish an analytical model of the biaxial test, determination of the parameters of the thermo-viscoplastic model is necessarily obtained by an inverse procedure coupling a FE model of the biaxial tensile test to a minimization algorithm of a cost function [8, 9]. In this procedure, the forces measured on each axis of the specimen are the input data of the FE model. The cost function to be minimized is established from the temporal evolution of the principal strains evaluated at the center of the specimen. More precisely, the cost function is calculated by the difference between calculated and experimental major and minor principal strains.

To avoid convergence problems during the numerical simulation from the FE model of the equi-biaxial tensile test, the different experimental operating conditions are simulated up to a final time corresponding approximately to the onset of necking (before strain localization appears). For this purpose, a simulation time corresponding to 85% of the experimental time to failure for each operating condition is chosen. Fig. 10 shows the post-treated experimental forces along the two specimen arms versus time curves

and principal strains at the specimen central point versus time curves for each experimental condition tested. This experimental database will be used in the identification procedure (see section 4) to calibrate the parameters of the material model which will be chosen in the next section.

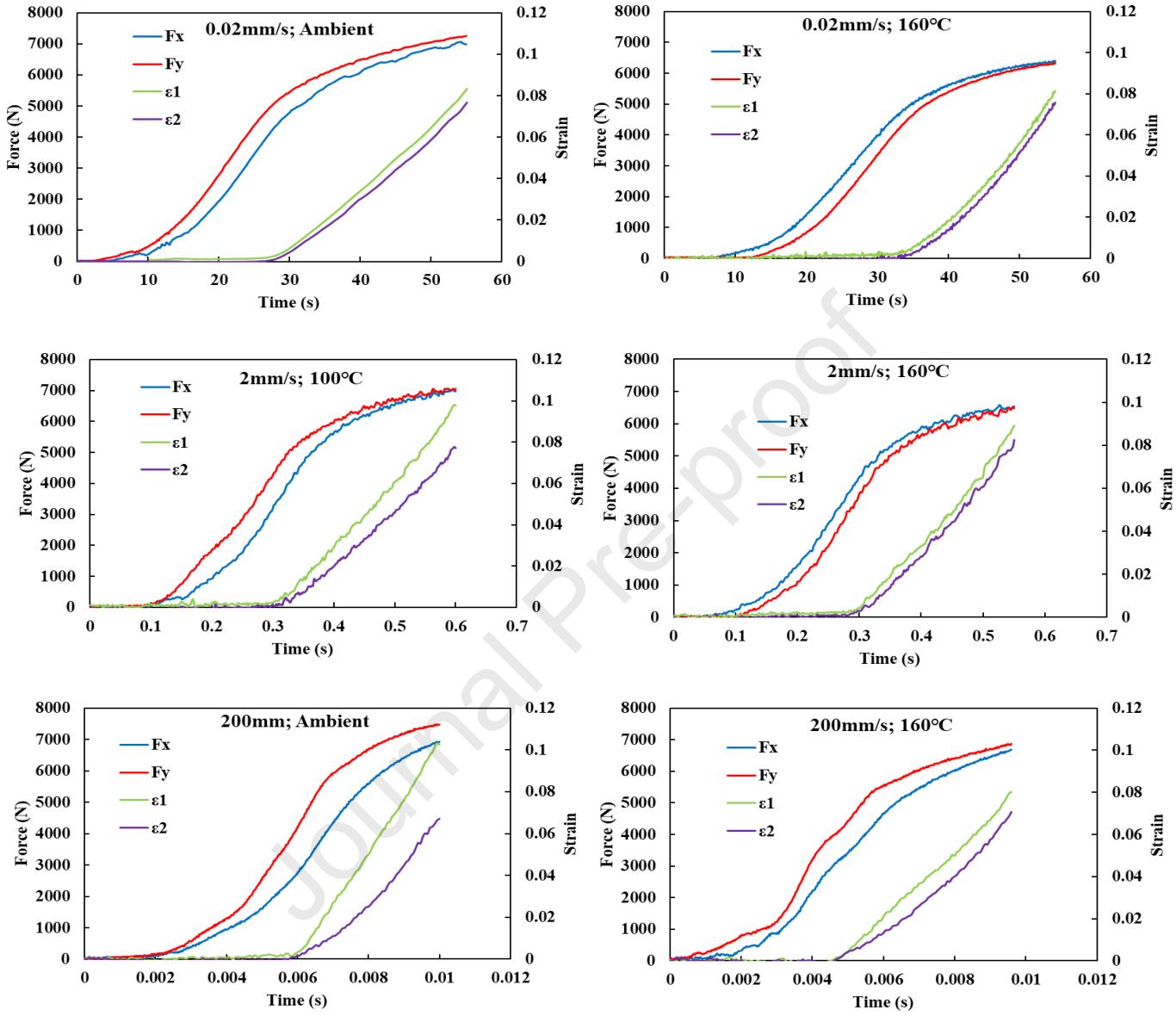

Fig. 10 Experimental forces and principal strains versus time curves for the identification stage.

3 Choice of a thermo-viscoplastic strain hardening model

The aim of the present work is to propose a method for calibrating thermo-viscoplastic work hardening laws for metallic materials subjected to biaxial loadings. In order to select an appropriate formulation for a strain hardening model, a preliminary study based on a campaign of uniaxial tensile tests [34], was first performed on an AA6061-O.

3.1 Uniaxial stress-strain curves

The sensitivity of the material's strain hardening to temperature and strain rate was evaluated through uniaxial tensile tests performed at the temperatures of 20°C, 150°C, and 200°C and tensile test velocities of 0.1, 10 and 200mm/s corresponding respectively to an initial strain rates of 0.002s^{-1}, 0.2s^{-1}, and 4s^{-1}. The evolutions of stress-strain curves for those different conditions are shown in Fig. 11. For a given tensile velocity, the temperature has a negative influence on the flow stress. The flow stress curves increase monotonically with the evolution of strain at temperatures below 150°C. For a temperature of 200°C, the flow stress curves

of 10mm/s and 200mm/s show a saturated state with increasing strain, as shown in Fig. 11d. The flow stress temperature sensitivity is more pronounced at low tensile speed than at high tensile speed. It can be explained by the strain rate compensation to the flow stress at high temperatures. Meanwhile, with the increasing temperature, a positive strain rate sensitivity to the flow stress is observed in Fig. 11d. Through the comparison, it is well established that the hardening behavior of AA6061-O exhibited significant dependency on the temperature and strain rate effect.

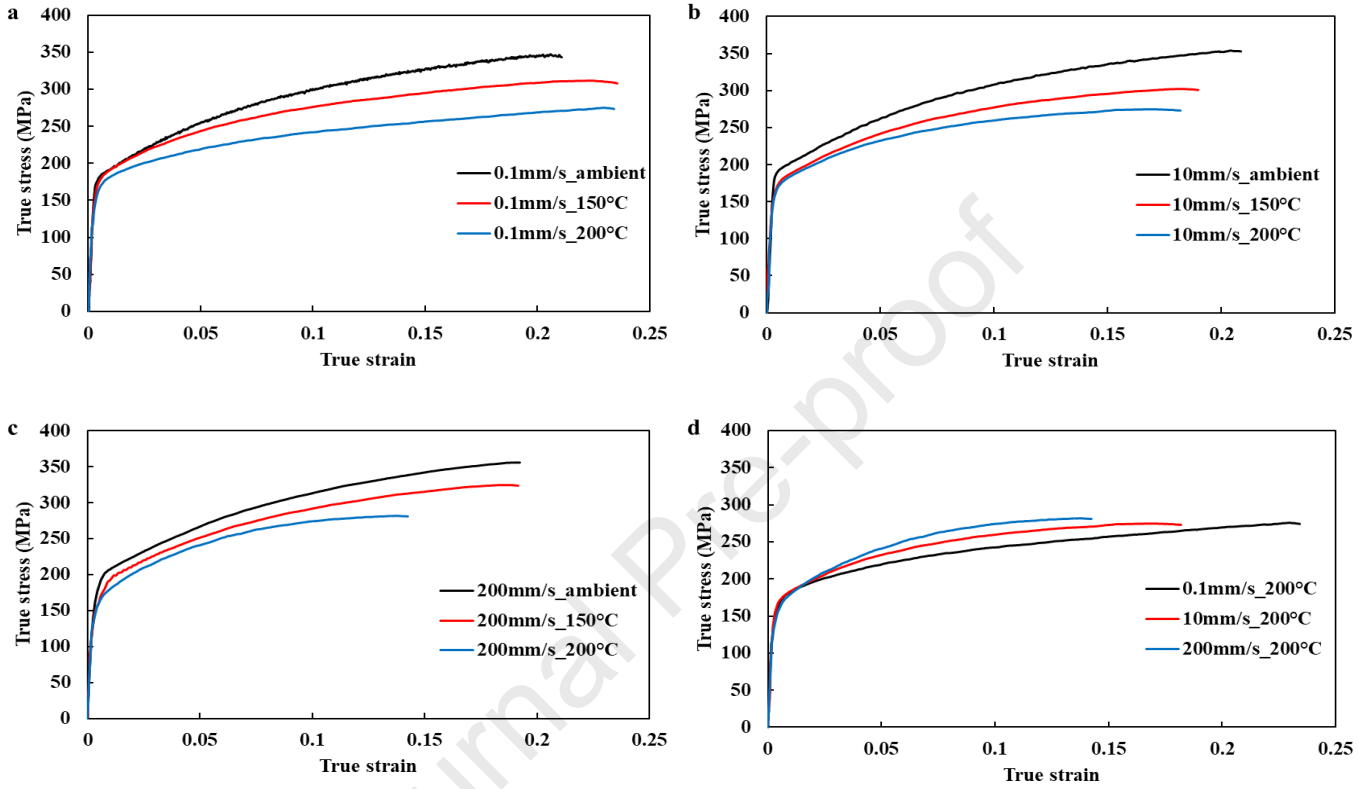

Fig. 11 Stress-strain curves at different temperatures and tensile speeds from uniaxial tensile tests [34].

3.2 Temperature and strain rate dependent hardening model

In the literature, FCC crystalline structures, including aluminum alloys, exhibit large hardening due to the amount of dislocation interactions with increasing strain [35]. The strain hardening tends to be highly temperature and strain rate dependent [36]. Chu et al. [38] investigated the hardening behavior of AA5086 in a range of temperatures (ambient to 200°C) and strain rates (0.01 to $2s^{-1}$) with different hardening models, which included the physical-based Zerilli-Armstrong (ZA) model and phenomenological models such as Ludwick (non-saturating) and Voce (saturating) models. Compared to the physical-based models, the phenomenological models have fewer parameters and are easier to calibrate and to integrate in commercial numerical simulation softwares. Based on previous work presented in [38], a Voce-type saturating model is chosen in this study to represent the strain hardening of the AA6061-O alloy in the temperature and strain rate ranges considered here. The parameters of this law are determined using an optimization method based on a gradient minimization function (Matlab software). This calibration approach is based on the analytical model of the tensile test considering the following assumptions: (i) homogeneity of the true-stress, true-strain and strain-rate fields in the sample gauged area, (ii) tests carried out under isothermal conditions and (iii) a constant strain rate equal to the initial one is assumed during the test.

The Voce's strain hardening law formulation is given by :

$$\bar{\sigma}=\sigma_0(T) + K_1\exp(-K_2T)\sqrt{1-\exp\left[-K_3\exp(K_4T)\bar{\varepsilon}_p\right]}\dot{\bar{\varepsilon}}_p^{\,m_0\exp(m_1T)} \quad (1)$$

where K_i and m_i are parameters to identify. The reference initial yield stress $\sigma_0(T)$ is expressed as :

$$\sigma_0(T) = \left\{1 - \frac{T}{T_m}\exp\left[K_0\left(1 - \frac{T_m}{T}\right)\right]\right\}\sigma_0(T_0) \quad (2)$$

where T is the current temperature, $T_m = 617°C$ is the melting temperature of the considered material and $\sigma_0(T_0) = 166.2\ MPa$ is the initial yield stress at ambient temperature. $K_0 = 0.2295$ is obtained by fitting the function $\sigma_0(T)$ (Eq. 2) on the experimental initial yield stresses at different temperatures as shown Fig. 12.

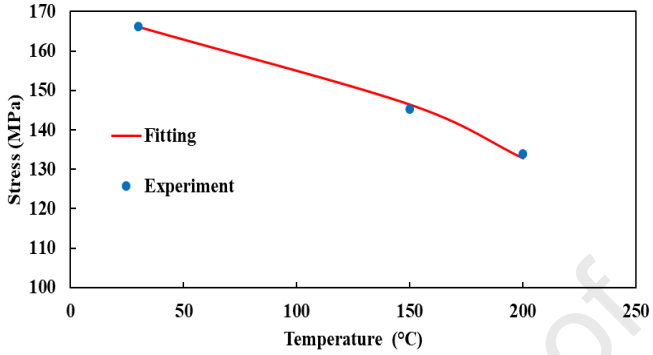

Fig. 12 Evolution of the initial yield stress for AA6061-O under uniaxial tension in function of the temperature.

From the experimental database composed of the true stress - equivalent plastic strain curves which are derived from the curves presented in Fig. 11, the Voce strain hardening law (Eq. 1) is identified. The parameters obtained are given in Table 2 below.

Table 2 Calibrated parameters for the Voce model.

K_1 (MPa)	K_2 (1/°C)	K_3	K_4 (1/°C)	m_0	m_1 (1/°C)	Cost function δ
334.2	0.00307	2.293	0.00633	0.00564	0.00811	1.8%

Fig. 13 compares the evolution of the predicted and experimental true stress versus equivalent plastic strain curves. Figure 13a, 13b and 13c were obtained from constant tensile test speeds of 0.1mm/s, 10mm/s and 200mm/s respectively, corresponding to initial strain rates of $0.002s^{-1}$, $0.2s^{-1}$ and $4s^{-1}$. The predicted curves, shown in Figure 13, are determined for constant strain rates during the test. This comparisons show that the selected model gives a good description of the AA6061-O strain hardening in the range of temperatures and strain rates tested. Therefore, this model will be selected to predict the strain hardening for different temperatures and strain rates under biaxial tensile conditions.

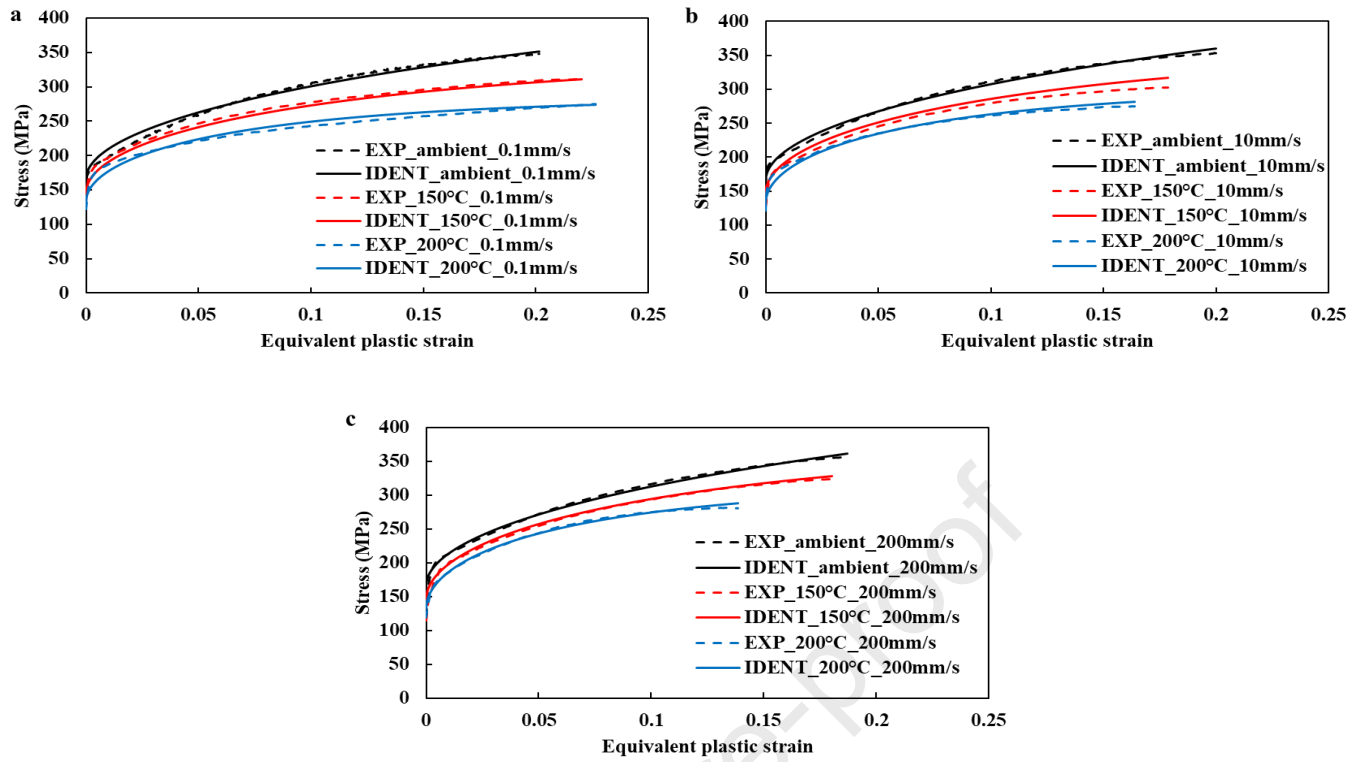

Fig. 13 Comparison of predicted and experimental true stress versus equivalent plastic strain curves.

4 Identification of hardening behavior under biaxial tension

4.1 Identification strategy

In this section, the hardening model chosen above is calibrated from biaxial tensile conditions presented Fig. 10.

The inverse procedure of parameter identification is presented in Fig. 14. This procedure is based on a finite element (FE) model of the in-plane biaxial tensile test applied on the cruciform specimen defined in Fig. 3. Temporal evolutions of experimental forces along the two axes of the specimen are introduced as boundary conditions in the FE model to simulate the biaxial tension test. At the end of the simulation, the numerical observable quantities are the principal strains at the central point of the specimen, whereas the experimental observables are the principal strains calculated by the DIC technique.

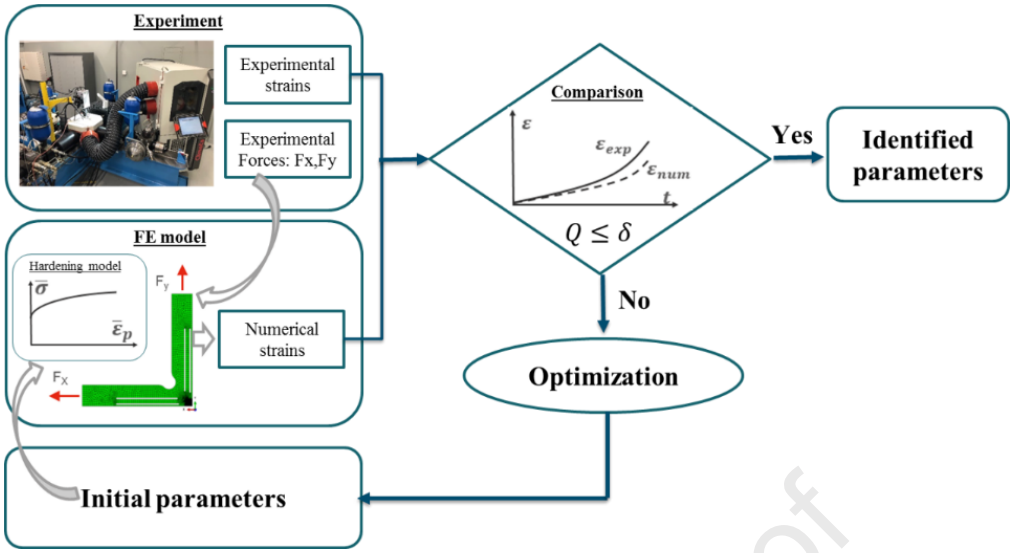

Fig. 14 Flowchart of parameter identification procedure.

By comparing the temporal evolutions of the experimental and numerical principal strains at the central point of the specimen, the cost function Q is calculated as follows:

$$Q = \frac{1}{p}\sum_{k=1}^{p} Q_k \quad \text{with} \quad Q_k = \frac{1}{2}\sum_{i=1}^{2}\sqrt{\sum_{j=1}^{q}\left(\varepsilon_i^{sim}(t_j) - \varepsilon_i^{exp}(t_j)\right)^2 / \sum_{j=1}^{q}\left(\varepsilon_i^{exp}(t_j)\right)^2} \tag{4}$$

where p is the number of experimental tests used for the identification procedure. As shown in figure 10, in this study, the experimental database includes 6 different operating conditions; q is the total number of time points during simulation; ε_1^{sim} and ε_2^{sim} are the major and minor numerical strains at the central point of the specimen; $\varepsilon_1^{\exp}$ and $\varepsilon_2^{\exp}$ are the experimental principal strains at the central point of the specimen.

The cost function Q is evaluated through an optimization loop built in the software platform ModeFRONTIER [39]. In order to make sure that the global minimum can be obtained, the MOGA (Multi-objectives Genetic Algorithm) method is firstly adopted to roughly determine the value area of parameters. Thereafter, the simplex method is applied for looking for the local minimum solution.

Based on a coupled temperature-displacement analysis, FE simulations of the biaxial tensile test at different loading conditions (temperatures: 20, 100, and 160 °C and tensile speeds: 0.02, 2, and 200 mm/s) are led. The model is based on a shell element mesh of the in-plane cross specimen. To keep reasonable simulation time, shell element mesh is preferred rather than 3D element mesh. This point is of paramount importance since this model is integrated next in an inverse procedure to identify material parameters. This procedure requires a number of FE simulations to determine the best set of material parameters of the thermo-viscoplastic model. The mesh of the specimen is shown in Fig. 15 (only one quarter due to symmetry). From a parametric study, Liu et al. [32] have defined the equivalent thicknesses of the different regions of the shell element mesh giving the same strain evolution in the central zone of the specimen than the one given by the 3D solid mesh. Zone A is the central flat thickness-reduced zone with the thickness of 0.625 mm, zone B is the transition zone with a thickness of 1.3125 mm, while zone C has the initial sheet thickness of 2 mm. Since the central zone is the zone of interest under biaxial tensile state, a refined mesh is defined in this area. Four nodes thermally coupled shell element (S4RT) are used for this model. For boundary conditions, sides 1 and 2 are symmetry axes. Experimental forces F_x and F_y are applied on sides 3 and 4 along axis X and Y, respectively.

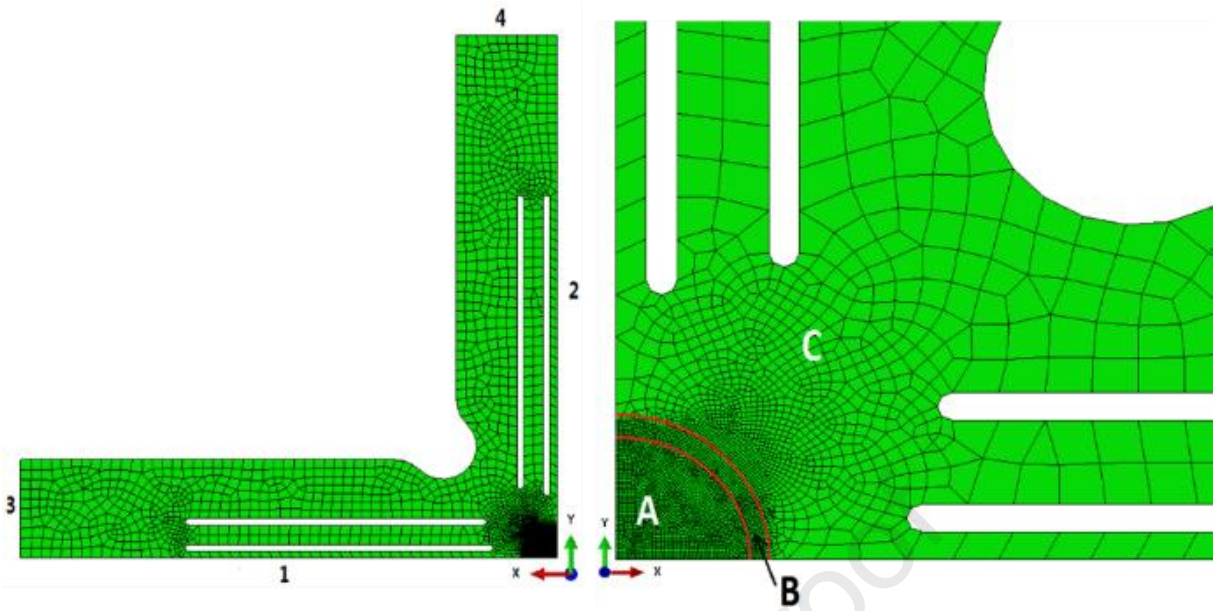

Fig. 15 Finite element mesh of the cruciform specimen.

The hardening law selected in section 3 is programmed through the user subroutine UHARD in the environment software ABAQUS. The Young's modulus (E = 63240 MPa) and the Poisson ratio (ν = 0.33) for AA6061-O were obtained in [34], which are assumed independent of the temperature and the strain rate. The thermal properties of AA6061-O adopted in simulations are presented in Table 3 [40].

Table 3 Material properties of AA6061-O [40].

Temperature $(°C)$	Thermal conductivity ($W.m^{-1}.K^{-1}$)	Heat capacity ($J.kg^{-1}.K^{-1}$)	Density ($kg.m^{-3}$)	Melting point $(°C)$
0	162	917		
98	177	978	2703	582-652
201	192	1028		

At the beginning of the simulation, a constant temperature (the set-point one) is assumed in the specimen. In these numerical simulations, adiabatic conditions are assumed, which means that no heat exchanges are considered between the specimen and the insulated box's environment and specimen grips. Even if this assumption is not rigorously verified, particularly for tests at the lowest speed (0.02mm/s), it enables the finite element numerical model used in the identification loop to be simplified and calculation times to be considerably reduced (furthermore, this assumption was also made in section 3 for the calibration of the work-hardening model based on uniaxial tests).

The initial yield stress is always assumed to evolve with temperature according to equation (2). The initial yield stress at ambient temperature $\sigma_0(T_0)$, with $T_0 = 20°C$, is identified along with the other hardening parameters for the different biaxial tensile conditions experimentally tested. In equation (2), the parameter $K_0 = 0.2295$ determined from uniaxial tensile conditions is always considered here for the identification stage under biaxial loadings since the temperature effect on the initial yield stress is assumed to be the same whatever the strain state.

4.2 Identification results

The identified parameters of the thermo-viscoplastic hardening model are shown in Table 4. As shown in Table 4, the initial yield stress estimated under biaxial tension ($\sigma_{0_biaxial} = 148.5$MPa) at room temperature is lower than the one obtained from uniaxial tension ($\sigma_{0_uniaxial} = 166$MPa) which confirms that this aluminum alloy does not exhibit isotropic plastic behavior, prohibiting any direct comparison between the two types of work hardening curve identified from either uniaxial or biaxial tests.

Table 4 Identified parameters for the Voce hardening model.

σ_0 (MPa)	K_1 (MPa)	K_2 (1/°C)	K_3	K_4 (1/°C)	m_0	m_1 (1/°C)
148.5	351.87	0.0036	1.039	0.0087	0.0024	0.013

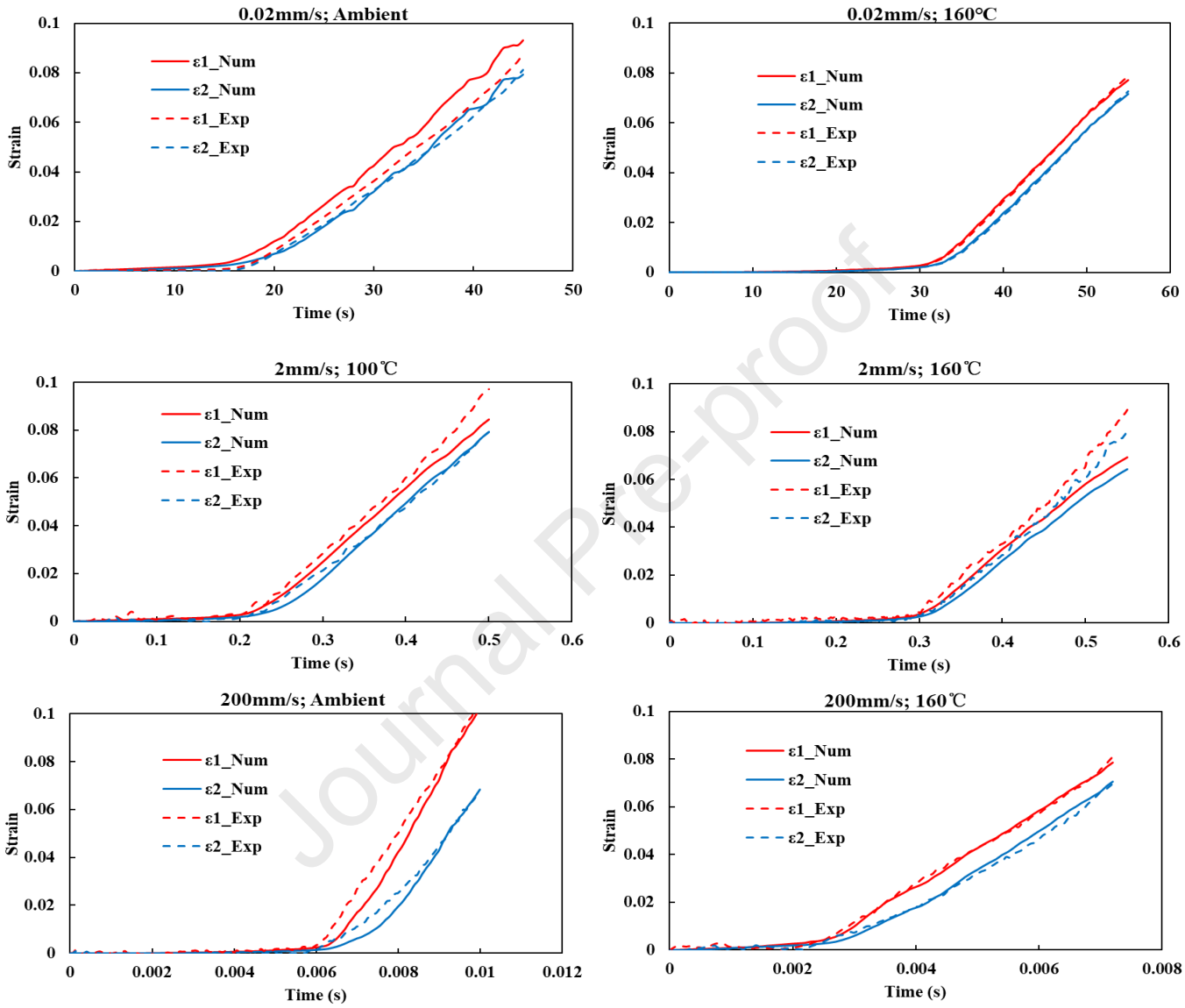

Fig. 16 Comparison of experimental and numerical temporal strain evolutions at the central point for different conditions.

The prediction of principal strains for the different conditions are compared with experimental data, as shown in Fig. 16. These comparisons show that the identified hardening model based on biaxial tensile tests, globally, well describe the evolution of principal strains in the range of temperatures and strain rates tested. For the tensile velocity of 2mm/s at 100°C and 160°C, the prediction of principal strains give an underestimation compared to the experimental data mainly at the end of the test for larger strains. For the tensile velocity of 200mm/s at 100°C and 160°C, this phenomenon has not been observed in terms of the strain rate compensation.

Flow stress predictions for large strains from the identified hardening model at different temperatures (ambient, 100°C, and 160°C) and strain rates ($0.001s^{-1}$, $0.1s^{-1}$, and $10s^{-1}$) are shown in Fig. 17. Constant temperatures and strain rates are introduced in these models and the equivalent stress is plotted up to an equivalent plastic strain of 40%. It can be seen that the predicted flow stresses decrease with the increase of temperature. A positive strain rate influence on the flow stress curves is observed at each temperature. With the increase of temperature, the strain rate effect becomes more significant with increasing plastic strain. Clearly,

implementing a calibration strategy for a strain-hardening model based on a non-homogeneous biaxial tensile test on a cruciform specimen is far less straightforward and more time-consuming than a simple calibration based on an analytical model. In addition to the fact that the biaxial tensile test achieves higher strain levels than those reached by a simple uniaxial tensile test, it has been shown in [39], that model calibration should be carried out on the basis of rheological tests involving strain states in the material as close as possible to those encountered in the forming process. For example, in [41], it was shown that calibration from a bulge test, inducing an equi-biaxial strain state, enables better estimation of forming forces in an incremental forming process.

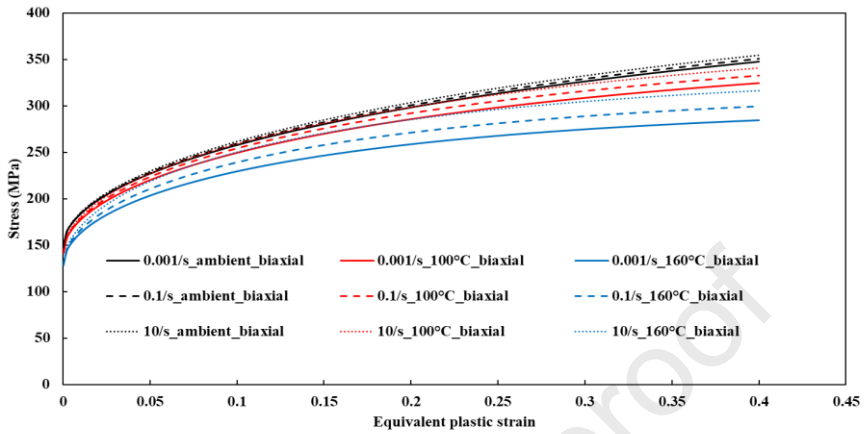

Fig. 17 Prediction of the identified hardening models from biaxial tensile tests at a large strains.

5 Conclusion

In this work, biaxial tensile tests have been performed on AA6061-O in-plane cross specimens in ranges of temperature from ambient to 160°C and strain rate from up to about $30s^{-1}$. The test bench used is equipped with an insulated box fed by an air flow generator to ensure a uniform temperature in the specimen at the beginning of the test. As expected, the experimental results show a negative effect of the temperature on the tensile strength while with respect to the strain rate, a negligible influence is observed for low temperatures (below 100°C) and a clear positive effect on the tensile strength is highlighted for higher temperatures (160°C in this study). Based on conventional uniaxial tensile tests performed in the same temperature and strain rate ranges as those targeted for the biaxial investigation campaign, a Voce formulation has been chosen to describe the sensitivities of strain hardening to temperature and strain rate. From an inverse procedure of calibration, the sensitivity of the AA6061 hardening behavior to the temperature and strain rate has been identified for large plastic strains under equi-biaxial loadings. In the temperature and strain rate ranges tested (temperature ranging from ambient to 160°C and strain rate from quasi-static condition $30s^{-1}$), the predicted strains at the cruciform specimen center obtained by the identified thermo-viscoplastic hardening model under biaxial tension show a relatively good agreement with experimental data. In future works, the calibration methodology of thermo-viscoplastic strain hardening models proposed here, based on biaxial tensile tests carried out over a limited temperature range (from ambient to 160°C), will be extended to characterizations at higher temperatures (up to 400°C), closer to those encountered in hot forming for aluminium alloys using induction heating device.

References

[1] Zhang S, Leotoing L, Guines D, Thuillier S, Zang S. Calibration of anisotropic yield criterion with conventional tests or biaxial test. International Journal of Mechanical Sciences 2014;85:142–51. https://doi.org/10.1016/j.ijmecsci.2014.05.020.

[2] Kuwabara T, Ikeda S, Kuroda K. Measurement and analysis of differential work hardening in cold-rolled steel sheet under biaxial tension. Journal of Materials Processing Technology 1998;80–81:517–23. https://doi.org/10.1016/S0924-0136(98)00155-1.

[3] Merklein M, Hußnätter W, Geiger M. Characterization of yielding behavior of sheet metal under biaxial stress condition at elevated temperatures. CIRP Annals 2008;57:269–74. https://doi.org/10.1016/j.cirp.2008.03.032.

[4] Naka T, Nakayama Y, Uemori T, Hino R, Yoshida F. Effects of temperature on yield locus for 5083 aluminum alloy sheet. Journal of Materials Processing Technology 2003;140:494–9. https://doi.org/10.1016/S0924-0136(03)00780-5.

[5] Naka T, Nakayama Y, Uemori T, Hino R, Yoshida F. Effect of Strain-Rate and Temperature on Yield Locus for 5083 Aluminum Alloy Sheet. KEM 2004;274–276:937–42. https://doi.org/10.4028/www.scientific.net/KEM.274-276.937.

[6] Teaca M, Charpentier I, Martiny M, Ferron G. Identification of sheet metal plastic anisotropy using heterogeneous biaxial tensile tests. International Journal of Mechanical Sciences 2010;52:572–80. https://doi.org/10.1016/j.ijmecsci.2009.12.003.

[7] Kulawinski D, Nagel K, Henkel S, Hübner P, Fischer H, Kuna M, et al. Characterization of stress–strain behavior of a cast TRIP steel under different biaxial planar load ratios. Engineering Fracture Mechanics 2011;78:1684–95. https://doi.org/10.1016/j.engfracmech.2011.02.021.

[8] Liu W, Guines D, Leotoing L, Ragneau E. Identification of sheet metal hardening for large strains with an in-plane biaxial tensile test and a dedicated cross specimen. International Journal of Mechanical Sciences 2015;101–102:387–98. https://doi.org/10.1016/j.ijmecsci.2015.08.022.

[9] Liu W, Guines D, Leotoing L, Ragneau E. Identification of strain rate-dependent mechanical behaviour of DP600 under in-plane biaxial loadings. Materials Science and Engineering: A 2016;676:366–76. https://doi.org/10.1016/j.msea.2016.08.125.

[10] Martins JMP, Andrade-Campos A, Thuillier S. Calibration of anisotropic plasticity models using a biaxial test and the virtual fields method. International Journal of Solids and Structures 2019;172–173:21–37. https://doi.org/10.1016/j.ijsolstr.2019.05.019.

[11] Yu Y, Wan M, Wu X-D, Zhou X-B. Design of a cruciform biaxial tensile specimen for limit strain analysis by FEM. Journal of Materials Processing Technology 2002;123:67–70. https://doi.org/10.1016/S0924-0136(02)00062-6.

[12] Zidane I, Guines D, Léotoing L, Ragneau E. Development of an in-plane biaxial test for forming limit curve (FLC) characterization of metallic sheets. Meas Sci Technol 2010;21:055701. https://doi.org/10.1088/0957-0233/21/5/055701.

[13] Leotoing L, Guines D, Zidane I, Ragneau E. Cruciform shape benefits for experimental and numerical evaluation of sheet metal formability. Journal of Materials Processing Technology 2013;213:856–63. https://doi.org/10.1016/j.jmatprotec.2012.12.013.

[14] Leotoing L, Guines D. Investigations of the effect of strain path changes on forming limit curves using an in-plane biaxial tensile test. International Journal of Mechanical Sciences 2015;99:21–8. https://doi.org/10.1016/j.ijmecsci.2015.05.007.

[15] Lee RS, Chien TW. A New Method for Testing Formability in Sheet Metal Forming at Biaxial Tensile State. KEM 2014;626:275–80. https://doi.org/10.4028/www.scientific.net/KEM.626.275.

[16] Song X, Leotoing L, Guines D, Ragneau E. Characterization of forming limits at fracture with an optimized cruciform specimen: Application to DP600 steel sheets. International Journal of Mechanical Sciences 2017;126:35–43. https://doi.org/10.1016/j.ijmecsci.2017.03.023.

[17] Xiao R, Li X-X, Lang L-H, Song Q, Liu K-N. Forming limit in thermal cruciform biaxial tensile testing of titanium alloy. Journal of Materials Processing Technology 2017;240:354–61. https://doi.org/10.1016/j.jmatprotec.2016.10.016.

[18] ISO 16842:2021. ISO n.d. https://www.iso.org/cms/render/live/en/sites/isoorg/contents/data/standard/08/20/82087.html (accessed July 12, 2022).

[19] Abu-Farha F, Hector LG, Khraisheh M. Cruciform-shaped specimens for elevated temperature biaxial testing of lightweight materials. JOM 2009;61:48–56. https://doi.org/10.1007/s11837-009-0121-8.

[20] Kulawinski D, Hoffmann M, Weidner A, Lippmann T, Lamprecht G, Henkel S, et al. Fatigue behaviour of 16Mo3 steel at elevated temperatures under uniaxial as well as biaxial-planar loading: Fatigue Behaviour of 16Mo3 Steel at Elevated Temperatures Under Uniaxial as Well as Biaxial-Planar Loading. Fatigue Fract Engng Mater Struct 2017;40:909–23. https://doi.org/10.1111/ffe.12551.

[21] Shao Z, Li N, Lin J, Dean TA. Development of a New Biaxial Testing System for Generating Forming Limit Diagrams for Sheet Metals Under Hot Stamping Conditions. Exp Mech 2016;56:1489–500. https://doi.org/10.1007/s11340-016-0183-9.

[22] Xiao R, Li X-X, Lang L-H, Chen Y-K, Yang Y-F. Biaxial tensile testing of cruciform slim superalloy at elevated temperatures. Materials & Design 2016;94:286–94. https://doi.org/10.1016/j.matdes.2016.01.045.

[23] Agarwal H, Gokhale AM, Graham S, Horstemeyer MF. Void growth in 6061-aluminum alloy under triaxial stress state. Materials Science and Engineering: A 2003;341:35–42. https://doi.org/10.1016/S0921-5093(02)00073-4.

[24] Dorbane A, Ayoub G, Mansoor B, Hamade R, Kridli G, Imad A. Observations of the mechanical response and evolution of damage of AA 6061-T6 under different strain rates and temperatures. Materials Science and Engineering: A 2015;624:239–49. https://doi.org/10.1016/j.msea.2014.11.074.

[25] Fan X, Suo T, Sun Q, Wang T. Dynamic mechanical behavior of 6061 al alloy at elevated temperatures and different strain rates. Acta Mechanica Solida Sinica 2013;26:111–20. https://doi.org/10.1016/S0894-9166(13)60011-7.

[26] Chen Z, Fang G, Zhao J-Q. Formability Evaluation of Aluminum Alloy 6061-T6 Sheet at Room and Elevated Temperatures. J of Materi Eng and Perform 2017;26:4626–37. https://doi.org/10.1007/s11665-017-2895-0.

[27] Khamei AA, Dehghani K. Effects of strain rate and temperature on hot tensile deformation of severe plastic deformed 6061 aluminum alloy. Materials Science and Engineering: A 2015;627:1–9. https://doi.org/10.1016/j.msea.2014.12.081.

[28] Kacem A, Laurent H, Thuillier S. Experimental and numerical investigation of ductile fracture for AA6061-T6 sheets at room and elevated temperatures. International Journal of Mechanical Sciences 2022;222:107201. https://doi.org/10.1016/j.ijmecsci.2022.107201.

[29] Rudnytskyj A, Simon P, Jech M, Gachot C. Constitutive modelling of the 6061 aluminium alloy under hot rolling conditions and large strain ranges. Materials & Design 2020;190:108568. https://doi.org/10.1016/j.matdes.2020.108568.

[30] Chu X, Leotoing L, Guines D, Ragneau E. Effect of Material Thermo-viscoplastic Modeling on the Prediction of Forming Limit Curves of Aluminum Alloy 5086. J of Materi Eng and Perform 2015;24:3459–70. https://doi.org/10.1007/s11665-015-1643-6.

[31] Zhang S, Léotoing L, Guines D, Thuillier S. Potential of the Cross Biaxial Test for Anisotropy Characterization Based on Heterogeneous Strain Field. Exp Mech 2015;55:817–35. https://doi.org/10.1007/s11340-014-9983-y.

[32] Liu W. Identification of strainrate dependent hardening sensitivity of metallic sheets under in-plane biaxial loading. These de doctorat. Rennes, INSA, 2015.

[33] Kim WJ, Yoo SJ. Enhanced ductility and deformation mechanisms of ultrafine-grained Al–Mg–Si alloy in sheet form at warm temperatures. Scripta Materialia 2009;61:125–8. https://doi.org/10.1016/j.scriptamat.2009.03.037.

[34] Liang J, Guines D, Leotoing L. Thermo-viscoplastic behavior of AA6061 under dynamic biaxial loadings: AIP Conference Proceedings: Vol 2113, No 1 n.d. https://aip.scitation.org/doi/abs/10.1063/1.5112752 (accessed July 12, 2022).

[35] Kocks UF, Mecking H. Physics and phenomenology of strain hardening: the FCC case. Progress in Materials Science 2003;48:171–273. https://doi.org/10.1016/S0079-6425(02)00003-8.

[36] Rusinek A, Rodríguez-Martínez JA, Arias A. A thermo-viscoplastic constitutive model for FCC metals with application to OFHC copper. International Journal of Mechanical Sciences 2010;52:120–35. https://doi.org/10.1016/j.ijmecsci.2009.07.001.

[37] Vilmosa V, Clausen AH, Borvik T, Holmedal B, Hopperstad OS. A physically-based constitutive model applied to AA6082 aluminium alloy at large strains, high strain rates and elevated temperatures. Materials & Design 2016;103:391-405. https://doi.org/10.1016/j.matdes.2016.04.047.

[38] Chu X. Caractérisation expérimentale et prédiction de la formabilité d'un alliage d'aluminium en fonction de la température et de la vitesse de déformation. phdthesis. INSA de Rennes, 2013.

[39] modeFRONTIER Simulation automation and design optimization. engineering.esteco.com.

[40] Seli H, Awang M, Ismail AIMd, Rachman E, Ahmad ZA. Evaluation of properties and FEM Model of the Friction welded mild Steel-Al6061-Alumina. Mat Res 2012;16:453–67. https://doi.org/10.1590/S1516-14392012005000178.

[41] Abdelkefi A, Guines D., Léotoing L, Thuillier S. Relevant material characterization for load prediction in incremental forming. International Journal of Material Forming (2022) 15:23. https://doi.org/10.1007/s12289-022-01676-6.

Identification of thermo-viscoplastic behavior for AA6061 under in-plane biaxial loadings

Highlights :

- Biaxial tests are performed on a specific in-plane cruciform specimen shape
- Thermo-viscoplastic strain-hardening of AA6061 is calibrated for large plastic strains
- Tests are carried out up to 200°C, for strain rates ranging from quasi-static to intermediate
- Thermo-viscoplastic hardening model is calibrated by means of an inverse procedure
- The hardening model is identified for an equivalent plastic strain level of up to 30%

Author Agreement Statement

We the undersigned declare that this manuscript is original, has not been published before and is not currently being considered for publication elsewhere.
We confirm that the manuscript has been read and approved by all named authors and that there are no other persons who satisfied the criteria for authorship but are not listed. We further confirm that the order of authors listed in the manuscript has been approved by all of us.
We understand that the Corresponding Author is the sole contact for the Editorial process. He/she is responsible for communicating with the other authors about progress, submissions of revisions and final approval of proofs

Signed by all authors as follows:

D. Guines

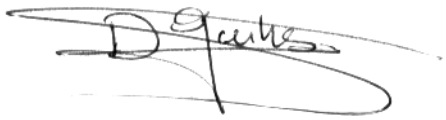

Declaration of interests

☒ The authors declare that they have no known competing financial interests or personal relationships that could have appeared to influence the work reported in this paper.

☐ The authors declare the following financial interests/personal relationships which may be considered as potential competing interests: